Impact Behavior of Hybrid Composite Plates

Metin Sayer, Numan Behlül Bektaş, Hasan Çallioğlu

Department of Mechanical Engineering, Pamukkale University, Denizli 20070, Turkey

Received 22 December 2008; accepted 7 March 2010
DOI 10.1002/app.32437
Published online 21 May 2010 in Wiley InterScience (www.interscience.wiley.com).

ABSTRACT: This experimental study deals with the impact response of hybrid composite laminates. Two different hybrid composite laminates, aramid/glass and aramid/carbon, and two different stacking sequences, such as $[0/0/90/90]_A+ [90/90/0/0]_G$ for AG1 and $[0/90/\pm45]_A+ [\pm45/90/0]_G$ for AG2 and so on (see Table I), were chosen for impact testing. The impact energy was gradually increased until complete perforation took place, and an energy profiling method (EPM) was used to identify the perforation thresholds of composites. The damaged samples were visually inspected. The images of the several samples subjected to various impact energies were registered and used for comparison and identifying damage mechanisms. The perforation thresholds for $[0/90/\pm45]_s$ aramid/glass and aramid/carbon laminates were found to be approximately 5% higher than those for their counterparts with the $[0/0/90/90]_s$ stacking sequence. © 2010 Wiley Periodicals, Inc. J Appl Polym Sci 118: 580–587, 2010

Key words: impact resistance; composites; failure; indentation

INTRODUCTION

Aramid fiber composites have been extensively utilized in many engineering applications, especially military helmets, body armor, land vehicles, and aviation industries, since they provide good damage tolerance, low density, and excellent impact resistance. These properties may be improved by hybridization, i.e., additional reinforcing with E-glass and carbon fibers. There has been a growing interest to examine impact response of both plain and hybrid composites.[1–6] Imielińska et al. have used air-coupled C-scan technique for defect size estimation in studies of impact and post-impact response of hybrid laminates for naval structures. They have shown that the presence of a polymer film on the sample surface can be useful in detecting the impact damage.[7]

Park and Jang have investigated the effect of stacking sequence and surface treatment on compression after impact performance of aramid fiber/glass fiber hybrid composites.[8] Gustin et al. have studied the impact, compression after impact, and tensile stiffness properties of sandwich composites including different combinations of carbon fiber and Kevlar® layers.[9] Park and Jang have prepared both one-layer and two-layer aramid fiber/PE fiber hybrid composites to compare the impact performance of interply and intraply hybrid composites. They have also investigated the impact damage mechanism of intraply hybrid composites with respect to load transfer at crossover points.[10]

Lim et al. have examined impact response of four-ply knitted Kevlar® fabric reinforced epoxy composites with three different stacking sequences.[11] Park and Jang have examined the effect of stacking sequence and surface treatment on delamination area of hybrid composites by using penetrant injection and de-plying technique.[12] Sugun and Rao have evaluated the low-velocity repeated impact response of advanced composites such as glass/epoxy, carbon/epoxy, and Kevlar®/epoxy.[13] Yao et al. have investigated the tensile, impact, and dielectric properties of five types of 3D orthogonal woven aramid-glass fiber/epoxy hybrid composites to show how the structural variation of the hybrid composites affected these properties.[14]

Wan et al. have studied the load–displacement behaviors, flexural, impact, and shear strength properties of 3D braided carbon/Kevlar® hybrid composites as a function of Kevlar®/carbon ratio. They have found that hybridization provided both higher flexural strength and modulus for the 3D braided composites.[15] Imielińska and Guillaumat have examined water immersion of two different woven glass–aramid-fiber/epoxy laminates and found that the load causing delamination and impact energy absorption were not significantly affected by the absorbed water.[16] Park and Jang have investigated the effect of position of the aramid layer on impact behavior of aramid fiber/glass fiber hybrid

Correspondence to: M. Sayer (msayer@pau.edu.tr).
Contract grant sponsor: DPT (State Planning Organization); contract grant number: 2006K120950.

TABLE I
Layer Configuration and Properties of the Hybrid Composite Laminates

Sample ID	Stacking sequence	Nominal thickness (mm)	Unit volume density (g/cm^3)
AG1	$[0/0/90/90]_A+ [90/90/0/0]_G$	2.4	1.416
AG2	$[0/90/\pm45]_A+ [\pm45/90/0]_G$	2.4	1.416
AC1	$[0/0/90/90]_A+ [90/90/0/0]_C$	2.7	1.407
AC2	$[0/90/\pm45]_A+ [\pm45/90/0]_C$	2.7	1.407

A, aramid fabric; G, glass fabric; C, carbon fabric.

composites using driven dart impact tester.[17] Wang et al. have studied the effect of fiber arrangement in 3D woven hybrid composites subjected to low velocity impact.[18]

In the present study, impact response of aramid/glass and aramid/carbon composite laminates is examined for various impact energy levels ranging from ~ 15–65 J. The effect of stacking sequences on impact behavior is also investigated. The perforation thresholds of hybrid composites are determined using the energy profiling method (EPM). The damage mechanisms are discussed considering obtained data points and images of the damaged samples taken from both the impacted and opposite (non-impacted) sides.

MATERIALS AND EXPERIMENTAL METHOD

Materials and fabrication of laminates

In this study, aramid fabric with 400 tows/m (Twaron® 1610 dtex) was supplied from Akzo, carbon fabric with 210 tows/m (Panex® 35) was supplied from Zoltek, and glass fabric with 410 tows/m (Metyx® 600 tex) was supplied from Telateks. The aramid/E-glass-epoxy and aramid/carbon-epoxy hybrid composite laminates were fabricated from unidirectional fabrics by the hand lay-up method at Izoreel Firm, in Izmir-Turkey. Three types of unidirectional fabrics were used in manufacturing: E-glass fabric (270 g/m^2), 50 K Carbon fabric (330 g/m^2), and aramid fabric (340 g/m^2). An epoxy resin matrix based on CY225 epoxy prepolymer and HY225 hardener (supplied from Huntsman) was used in the production of the composite laminates. The mixing ratio for resin-to-hardener in weight was 10 : 2 and fiber volume fraction in all laminates was about 60%. The two stacking sequences that were chosen, other composite laminate' properties, and sample acronyms, are given in Table I. The hybrid composite laminates were cured in a lamination press for 2 h, at 120°C, at a constant pressure of 0.3 MPa. The composite laminates were then cooled down to the room temperature maintaining the pressure. Composite specimens with dimensions of 10 × 10 cm^2 were cut from the fabricated composite plates.

Impact testing

An Instron®-Dynatup® 9250 HV model instrumented drop weight impact testing machine was used for impact testing. It consists of a dropping crosshead with its accessories, a pneumatic clamping fixture, a pneumatic rebound brake, and Dynatup® 930-I impulse data acquisition system. The weight of crosshead can adjustable with drop mass and tup of the impactor has a 12.5 mm diameter hemispherical tip. Impulse data acquisition system records the electronic signals and converts them into the impact parameters. The total mass of the impactor was ~ 6.32 kg for all tests.

In this study, two different stacking sequences were chosen to investigate the impact response of both aramid/E-glass and aramid/carbon hybrid composite laminates subjected to increasing impact energy. The impact energies ranged from ~ 15–65 J, and tests were conducted up to complete perforation of the specimens. The perforation threshold can be defined as the minimum energy level at which the impactor passes through the thickness of the specimen, resulting in a permanent catastrophic damage to the specimen. With this use of increasing impact energies, it was possible to examine the damage process and impact response of aramid composite laminate until perforation of specimen.

RESULTS AND DISCUSSION

In the following paragraphs, force-deflection curves for the investigated composites and variation of impact parameters such as normalized (dimensionless) peak force and deflection values, and the effect of the stacking sequence are discussed. In addition, several images of damaged samples and damage mechanisms are also presented.

Contact force-deflection (F-d) curves

The contact force-deflection (F-d) curves give significant information regarding the impact behaviors of hybrid laminates during an impact event. The absorbed energy can be calculated from the area under the contact force-deflection curve. For comparison, only the contact force-deflection curves of composites for an impact energy of 30 J are shown in Figure 1. For the intended purpose, there is no need rather than to present the contact force-deflection curves for all tested impact energy values. As seen in the figure, curves have an ascending loading section up to a maximum contact force (peak force) followed by a descending unloading section. The

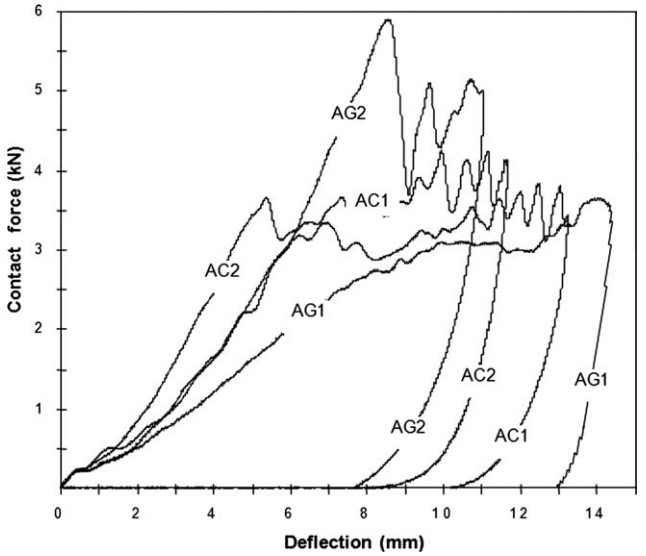

Figure 1 Contact force-deflection (F-d) curves of hybrid composites for impact energy 30 J.

ascending section of contact force-deflection curve is due to the resistance of composite to the impact loading and its slope reflects the composite bending stiffness. As the impactor makes contact with composite specimens, ascending section of contact force-deflection curves increase significantly, except for AG1. It is seen from this figure that samples AG2, AC1, and AC2 exhibit steeper initial slope compared to sample AG1. Additionally, sample AG1 has the highest deflection value while AG2 has the highest peak force value, for an impact energy 30 J. The last section of contact force-deflection curves represents impactor rebounding from specimen surface.

It can also be seen in Figure 1 that AC1 and AC2 have similar characteristics in terms of bending stiffness, peak force, and deflection in spite of slight differences. But, the AC1 hybrid composite exhibits an extended ascending section in the contact force-deflection curve when compared to the AC2 curve. A plateau occurs on the contact force-deflection curves when the impactor reaches the carbon layers. This plateau in the contact force-deflection curves represent reduction in stiffness of the hybrid composites, implying there is more damage accumulation in the carbon layers.

When contact takes place with the AG2 specimen, the contact force-deflection curve exhibits a linear increase and then reaches a peak force value (Fig. 1). When the nose of impactor reaches the glass layers, the contact force decreases suddenly and is followed by successive raise-drop sequences. So, it can also be deduced from the contact force-deflection curves that damage growth in glass layers causes the stiffness reduction. However, the bending stiffness and the peak force value for AG1 are considerably smaller compared to the others, while the deflection is higher. Apparently, due to unstable glass-fibers breakage occurring in inner layers and also the effect of stacking sequence, contact force-deflection curves of AG1 exhibit considerable higher deflections. As a result, the damaged AG1 composite absorbs more impact energy compared to the other investigated hybrid composites.

Impact characteristics

The contact force, deflection, and contact duration are important impact characteristics of the hybrid composites subjected to impact loading. For better understanding the impact behavior of the studied hybrid composites, plots of the impact characteristics versus impact energy, and the value of impact velocity at perforation are given in Figure 2.

In Figure 2(a), the peak contact force value versus impact energy is depicted. In general, in spite of small variations in peak force-impact energy curves, all are essentially horizontal. It seems that, all peak contact force values of AG2 are higher than those of the other hybrid composites. As the impact energy reaches the perforation threshold, hybrid composites show the maximum peak force value. Afterwards, peak force values for all hybrid composites decrease, as seen in Figure 2(a).

Figure 2(b) shows the variation of the deflection with impact energy for all hybrid composites. The deflection values of composites rapidly increase as the impact energy increases up to the perforation threshold. In general, the deflection values of AG1 hybrid composite are higher than those of the other hybrid composites, and AG1 hybrid composite has the maximum deflection value at the perforation threshold. After reaching perforation threshold, the maximum deflection values remain nearly constant for all hybrid composites.

The contact duration between impactor and hybrid composites versus impact energy, is shown in Figure 2(c). The contact duration values of hybrid composites increase with increasing impact energy. The contact duration values of AG1 hybrid composite are consistently higher than those of the other hybrid composites. For all hybrid composites, the highest contact durations are reached right before onset of perforation associated impact energies. Once perforation impact energy is attained, a sudden decrease occurs in contact duration for all hybrid composites. Additionally, it seems that contact durations for $[0/0/90/90]_s$ aramid/glass and aramid/carbon laminates are higher than those for their counterparts with $[0/90/\pm45]_s$ layups.

The impact velocity at perforation threshold is given in Figure 2(d). The impact velocity increases with increasing the impact energy. Since the perforation threshold energy of the AC2 hybrid composite

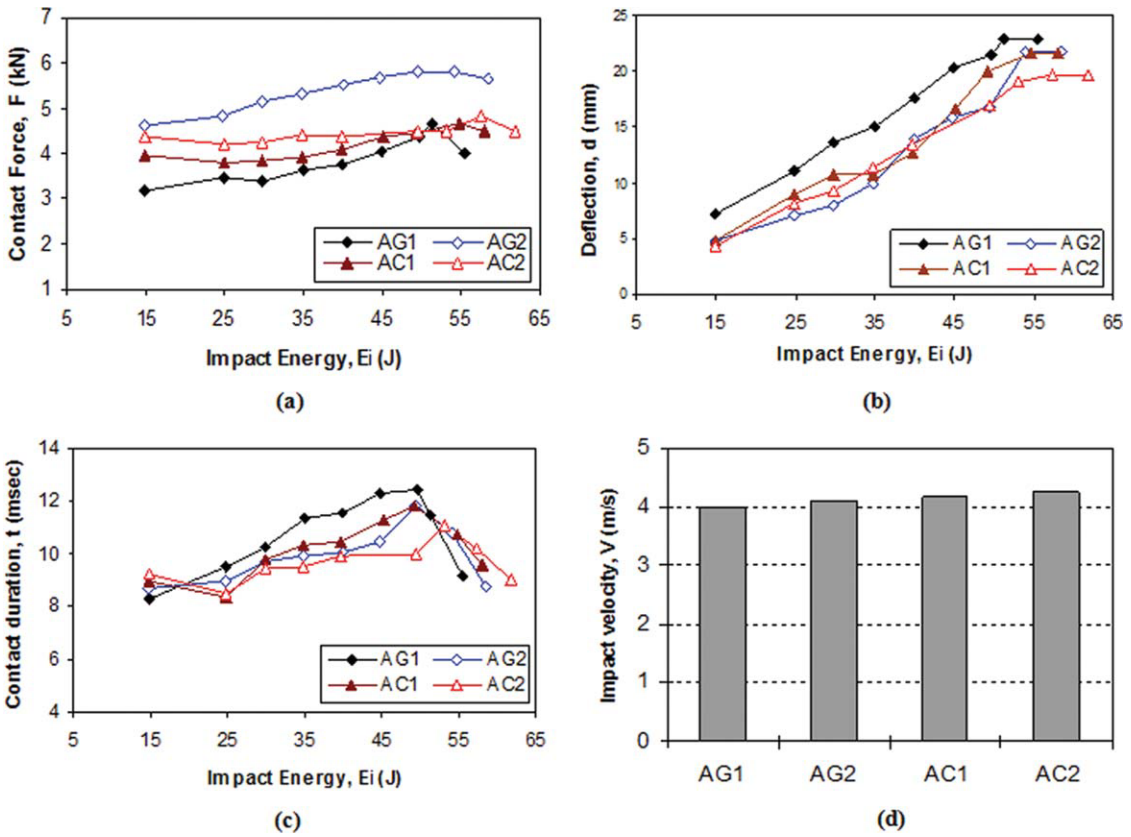

Figure 2 Variations of (a) contact force, (b) deflection, (c) contact duration versus impact energy (E_i), and (d) impact velocity at perforation threshold. [Color figure can be viewed in the online issue, which is available at www.interscience.wiley.com.]

is higher than that of the other hybrid composites, AC2 presents the highest impact velocity when the impact energy reaches the perforation threshold.

As can be seen in Figure 2(a,d), when the impact energy reaches the perforation threshold, impact parameters such as contact force and deflection attain their maximum values. Such maximum values for impact parameters of hybrid composites are summarized in Table II. Since the absorbed energy increases with increasing impact energy, when the impact energy reaches the perforation threshold, absorbed energy arrives at its maximum value. Therefore, maximum absorbed energy is determined by the perforation threshold.

As indicated in Table I, AG and AC samples are of the different thicknesses, i.e., 2.4 mm and 2.7 mm, respectively. To account for the thickness effect, impact parameters may be given an alternate form for a more accurate comparison. Therefore, Figure 3(a,b) summarize such peak force and deflection related values for the hybrid composites. The calculation process involved in obtaining the alternate quantities is performed as follows.

In the case of the peak force values, it can be considered appropriate calculating a value proportional to bending stress. For this, F^* is obtained with dividing the peak force by the square of thickness, ($F^* = F_{max}/t^2$). On the other hand, to compare deflection values, it is considered adequate calculating a quantity proportional to extension. This can be done by multiplying deflection with laminate thickness, ($d^* = d.t$). The effect of stacking sequences on the related

TABLE II
Impact Parameters of Hybrid Composites

	Peak force F_{max} (kN)	Total deflection d (mm)	Contact duration, t (ms)	Absorbed energy, E_a (J)	Perforation threshold, P_r (J)
AG1	4.63	22.97	12.43	51.05	51.22
AG2	5.82	21.81	11.83	53.40	54.01
AC1	4.64	21.56	11.80	54.06	54.70
AC2	4.81	19.75	11.07	57.36	57.42

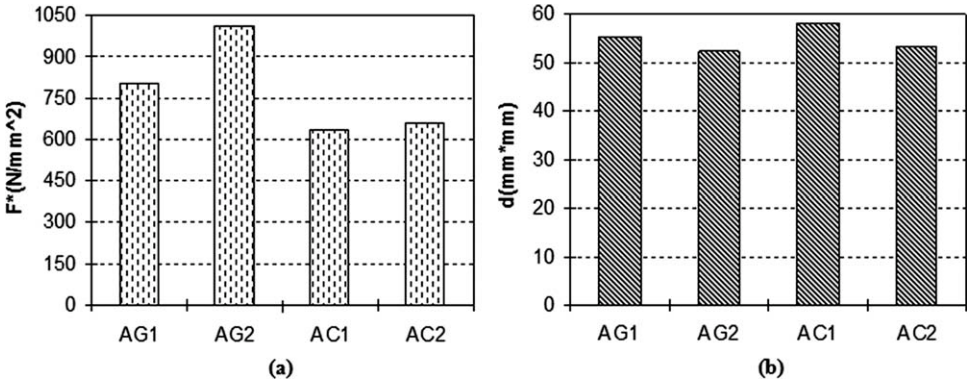

Figure 3 Comparison of (a) related peak force values and (b) related deflection values.

peak force and related deflection can also be seen from Figure 3(a,b). It seems that higher related peak force occurs for AG2 and AC2 with $[0/90/\pm45]_s$ layups compared to AG1 and AC1 with $[0/0/90/90]_s$ layups, implying higher stiffness of $[0/90/\pm45]_s$. On the contrary, related deflections for AG1 and AC1 compared to AG2 and AC2 are of higher values. Apparently, related deflection value of AC1 sample is the highest, as seen in Figure 3(b). That is, higher stiffness implies lower deflection, as expected.

Energy profile and failure mechanisms

The impact energy and absorbed energy are two main parameters to evaluate the impact response of composite laminates. The impact energy (E_i) can be defined as the energy introduced to a specimen from the impactor during an impact event. The absorbed energy (E_a) is defined as the entire energy absorbed by the specimen at the end of an impact event. The relationship between impact energy and corresponding absorbed energy can be shown in a diagram called as energy profile.[19] With determination of penetration and perforation thresholds, this is a useful method to create a correlation between impact energies and damage mechanisms.

According to test results, energy profile diagrams of AG and AC hybrid composites are depicted in Figure 4(a,b). The energy profile diagrams show the correlation between the impact energy and corresponding absorbed energy. A diagonal line, called equal-energy line, is added to diagrams representing the equality between impact and absorbed energies.

In Figure 4(a), energy profile diagrams of AG1 and AG2 hybrid composites are depicted. It is seen from the figure that for a given impact energy value, up to energy level of 35 J, the data points of AG1 are closer to the equal energy line than those of AG2. Therefore, the energy absorption capability of AG1 hybrid composite seems to be higher than that

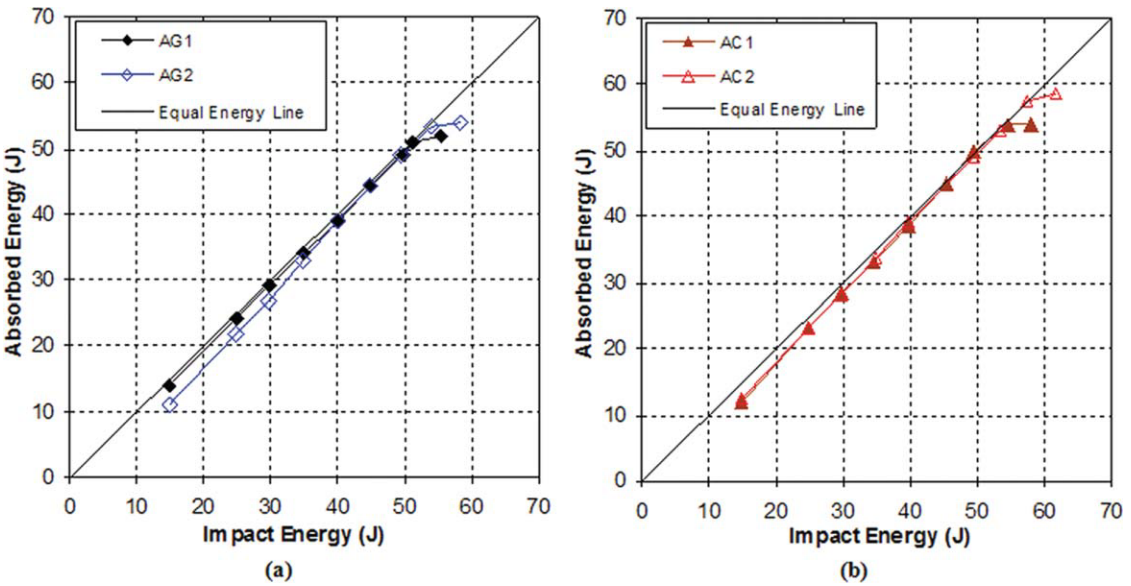

Figure 4 Energy profile diagrams of hybrid composites (a) AG1 and AG2 and (b) AC1 and AC2. [Color figure can be viewed in the online issue, which is available at www.interscience.wiley.com.]

of the AG2. Accordingly, the excessive impact energy (the difference between impact energy and corresponding absorbed energy) of AG1 hybrid composite is lower than that of the AG2 hybrid composite. The excessive impact energy is retained in the impactor and used to rebound the impactor from the sample at the end of an impact event.[20]

After this energy level, both stacking sequences have nearly the same energy absorption values up to the perforation. However, AG2 seems to have a higher perforation threshold. The perforation thresholds are determined approximately as 51.22 J for AG1 and 54.01 J for AG2. It is indicated in the former studies[21] that once perforation took place, independently of the impact energy, the absorbed energy value remains quite constant. Therefore, impact tests are not done beyond perforation threshold in this study.

As for the AC specimens, Figure 4(b), both stacking sequences, $[0/90/\pm45]_s$ and $[0/0/90/90]_s$, seem to have close energy absorption capacity up to perforation. Accordingly, the excessive impact energy values of samples are approximately equal for AC samples. However, as is in AG specimens, the $[0/90/\pm45]_s$ layup has higher perforation threshold. The perforation thresholds are determined approximately as 54.70 J for AC1 and 57.42 J for AC2. As a result, AC2 samples exhibited superior perforation threshold performance compared to all other types of hybrid composites, since it has the highest perforation threshold value.

Each fiber has different mechanical properties. Hence, using different fibers in the composition of hybrid composites results in different impact responses and damage modes. For fiber reinforced composites undergoing impact, the main energy absorption mechanism is delamination for aramid reinforced composites, while it is fiber breakage for glass and carbon reinforced composites. In general, for lower impact energies, i.e., until $E_i = 35$ J, impact events contain partial rebounding of impactor and damage concentrates at the impact contact point. After this energy level, the main damage modes are fiber breakage and expanding delamination between adjacent layers.

In what follows, some images of damaged samples are given for comparison. The photographs are taken from both the impacted and opposite (non-impacted) sides of the samples. When impact contact takes place, some delamination occurs at the bottom side of glass and carbon layers. Before taking photographs of damaged samples, these delaminated parts of bottom layer were removed to observation of interior layers. In addition to surface visual inspection, cross-sections of some damaged specimens were also examined to observe damage between adjacent aramid/glass or aramid/carbon interfaces. The photographs of damaged samples are presented in Figures 5 and 6.

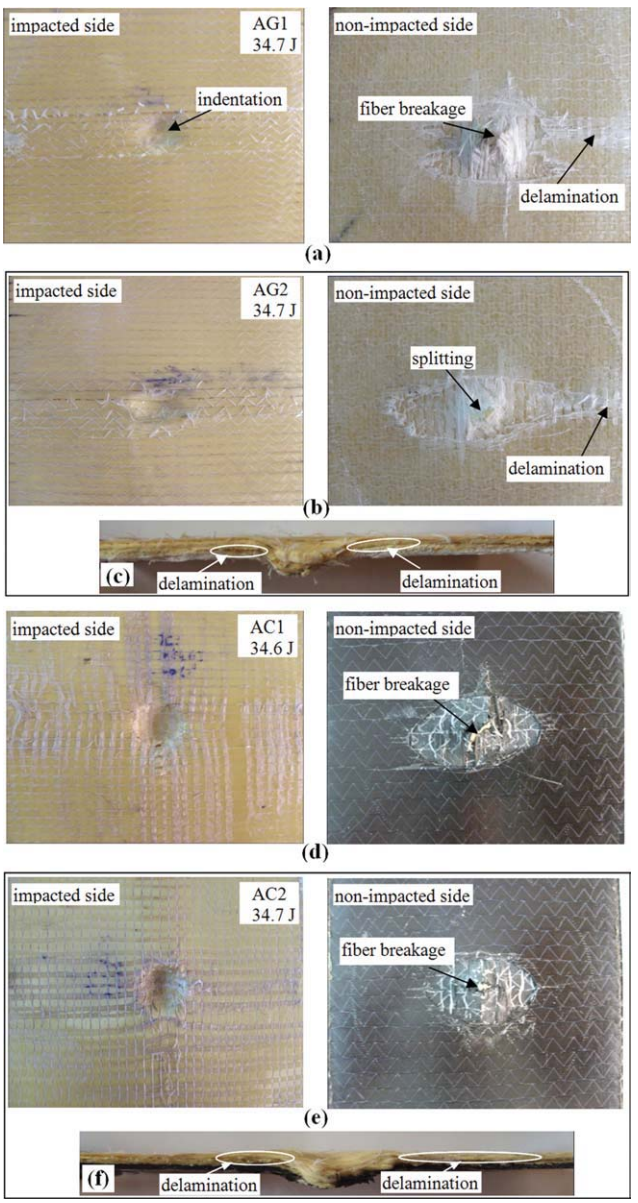

Figure 5 The photographs of damaged samples for lower impact energy. [Color figure can be viewed in the online issue, which is available at www.interscience.wiley.com.]

For lower impact energies (up to $E_i = 35$ J), the main damage mode is indentation and damage concentrates at the impact contact point. As can be seen from the front side of samples in Figure 5, indentation and related aramid fiber crushing took place, and some aramid fibers pulled out from the matrix right under the impact contact point. As can be seen from the back side of samples, splitting among glass fibers and fiber breakages started to take place. And also, some glass and carbon fibers were fractured through the thickness due to the tup nose reaching up to but not across the last lamina (Fig. 5). Consequently, at the bottom layer some carbon fiber pull-

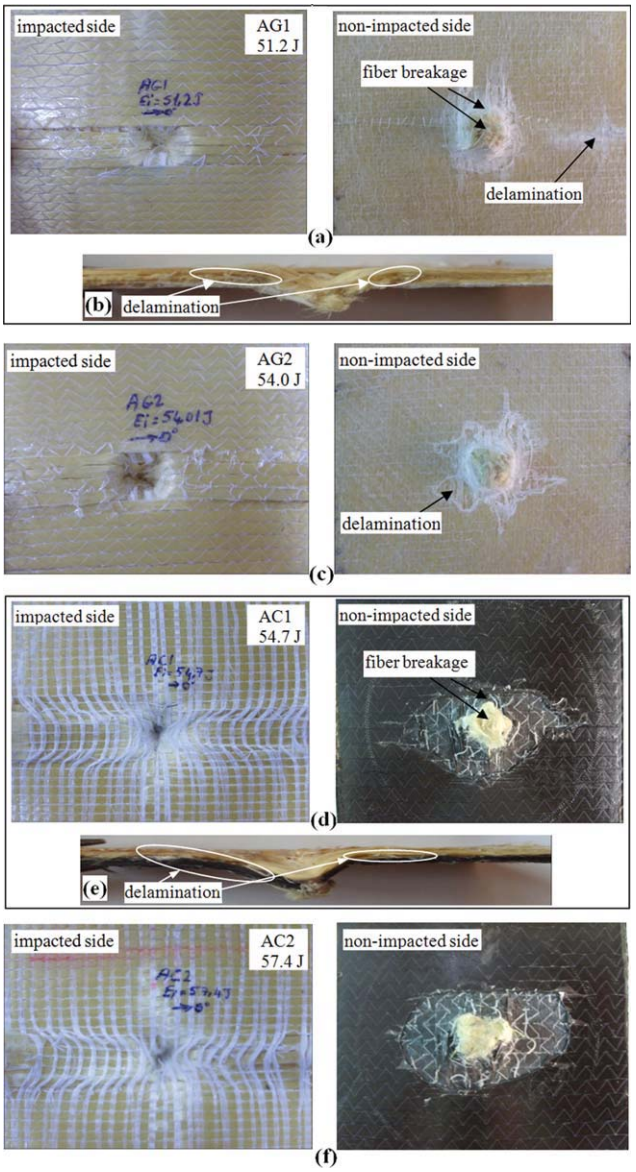

Figure 6 The photographs of damaged samples for perforation threshold. [Color figure can be viewed in the online issue, which is available at www.interscience.wiley.com.]

out from matrix took place for AC samples, while some glass fiber fracture and delamination happened for AG samples. Besides this, it seems that there is no further delamination in interior layers. When glass or carbon fibers are at the back surface of hybrid composites, these fibers restrict the extent of delamination in aramid layers. Because of the brittle properties of glass and carbon fibers, local damage occurs preferentially in layers containing these fibers, as seen from the back side of samples. However, for carbon layers more severe local damage occurred compared to glass layers, as seen from the back side of samples in Figure 5.

In Figure 5(c,f) of cross-sections of AG2 and AC2, it is observed that due to bending and indentation, some delamination took place between aramid layers and between aramid/glass and aramid/carbon interfaces. It appears that the extent of delaminated area between aramid fibers and adjacent aramid/carbon interfaces is bigger for AC2 than for AG2.

As the impact energy continued to increase until perforation threshold of composites, the size and extent of damage increased at all plies. Up to perforation threshold energy level, fiber breakage was recognized as the dominant damage mode for all hybrid composite samples. For this damage mode, the amount of damaged aramid fibers increased progressively along the thickness as the impactor nose penetrated more into the samples. The glass and carbon fibers were also damaged and fractured through the thickness at the back side. In this way, force-deflection curve of composites expands along the deflection axis and damaged composites absorb increasing impact energy.

When the impact energy further increases, perforation takes place for both AG and AC hybrid composites. As seen from Figure 4(a,b), when the impact energy value reaches the last data point on the equal energy line, perforation occurs for all hybrid composite samples. After this energy level, the impactor does not cause any more damage to the composite sample. Instead, only additional friction between the impactor and specimen occurs in what is called post-perforation frictional process.

Figure 6(a,f) show some images of damaged hybrid composites corresponding to the impact energy level of perforation. From the pictures, it is clearly seen that fiber breakage follows indentation at the point of impact. As contact progresses, aramid fibers were pulled out from the top lamina of specimen and pushed across the laminate thickness to the last lamina by the impactor nose. The perforated specimen figures indicate that fibers were fractured throughout all thickness length and the impactor nose merged out from the back side of the specimen when impact energy reached the composites perforation threshold. From the photographs of back side of specimens, catastrophic damages in both aramid/glass and aramid/carbon samples can be easily seen.

As seen in the photographs for back sides of samples, all glass and carbon fibers were completely fractured. Additionally, minor delaminations at the bottom layer of AG samples can be seen to occur at naked eye. It seems that the extents of delaminated areas for AC samples are bigger than those of the AG samples.

CONCLUSIONS

In this experimental study, impact behavior of aramid/glass and aramid/carbon hybrid composites

subjected to increasing impact energies has been studied. The following conclusions can be drawn from the tests:

- As the impact energy reaches the perforation threshold, impact parameters reach the maximum values with the exception of contact duration. The contact duration attains the highest value right before perforation. Once perforation takes place contact duration shows a sudden drop.
- It is shown that the related peak forces for $[0/90/\pm45]_s$ aramid/glass and aramid/carbon laminates are higher than those for their counterparts with the $[0/0/90/90]_s$ layups. On the contrary, related deflections for $[0/0/90/90]_s$ aramid/glass and aramid/carbon laminates according to theirs $[0/90/\pm45]_s$ layups are higher.
- For lower impact energies, impact events contain partial rebounding of impactor and damage concentrates at the contact-impact point, i.e., until $E_i = 35$ J. With a close examination of the samples, aramid fiber crushing related indentation took place at the impacted side while glass and carbon fiber breakage started to take place at the non-impacted side of the samples. However, fiber failures and delaminations between adjacent layers were observed to be the dominant damage mode at the non-impacted side when the impact energy increased.
- The stacking sequence seems to play an important role in impact response of composite laminates. It is observed that the perforation thresholds for $[0/90/\pm45]_s$ aramid/glass and aramid/carbon laminates were found to be $\sim 5\%$ higher than those for their counterparts with the $[0/0/90/90]_s$ stacking sequence.
- It seems from the energy profile diagrams that the energy absorption capability of AG1 hybrid composite seems to be higher than that of the AG2. Accordingly, the excessive impact energy of AG1 hybrid composite is lower than that of the AG2 hybrid composite.
- From energy profiles of the AC specimens, both stacking sequences $[0/90/\pm45]_s$ and $[0/0/90/90]_s$ seem to have close energy absorptions up to the perforation. Accordingly, the excessive impact energy values of samples are approximately equal for AC composites.

References

1. Abrate, S. Impact on Composite Structures; Cambridge University Press: Cambridge, 1998.
2. Zhu, G.; Goldsmith, W.; Dharan, C. K. H. Int J Solids Struct 1992, 29, 399.
3. Kang, T. J.; Kim, C. Polym Polym Compos 1997, 5, 265.
4. White, D. M.; Taylor, E. A.; Clegg, R. A. Int J Impact Eng 2003, 29, 779.
5. Kang, T. J.; Kim, C. Compos Sci Technol 2000, 60, 773.
6. Onal, L.; Adanur, S. J Ind Text 2002, 31, 255.
7. Imielińska, K.; Castaings, M.; Wojtyra, R.; Haras, J.; Le Clezio, E.; Hosten, B. J Mater Process Technol 2004, 157–158, 513.
8. Park, R.; Jang, J. Polym Compos 2000, 21, 231.
9. Gustin, J.; Joneson, A.; Mahinfalah, M.; Stone, J. Compos Struct 2005, 69, 396.
10. Park, R.; Jang, J. J Appl Polym Sci 2000, 75, 952.
11. Lim, C. T.; Tan, V. B. C.; Ramakrishna, S.; Lee, J. B. K. J Reinf Plast Compos 2002, 21, 121.
12. Park, R.; Jang, J. J Compos Mater 2000, 34, 1117.
13. Sugun, B. S.; Rao, R. M. V. G. K. J Reinf Plast Compos 2004, 23, 1583.
14. Yao, L.; Wenbin, L.; Wang, N.; Wang, L.; Guo, X.; Yiping, Q. J Mater Sci 2007, 42, 6494.
15. Wan, Y. Z.; Chen, G. C.; Huang, Y.; Li, Q. Y.; Zhou, F. G.; Xin, J. Y.; Wang, Y. L. Mater Sci Eng A 2005, 398, 227.
16. Imielińska, K.; Guillaumat, L. Compos Sci Technol 2004, 64, 2271.
17. Park, R.; Jang, J. Polym Compos 2001, 22, 80.
18. Wang, X.; Hu, B.; Feng, Y.; Liang, F.; Mo, J.; Xiong, J.; Qiu, Y. Compos Sci Technol 2008, 68, 444.
19. Liu, D.; Raju, B. B.; Dang, X. Int J Impact Eng 2000, 24, 733.
20. Liu, D. J Compos Mater 2004, 38, 1425.
21. Atas, C.; Liu, D. Int J Impact Eng 2008, 35, 80.